The Arg/N-degron pathway targets transcription factors and regulates specific genes

Tri T. M. Vu[a], Dylan C. Mitchell[b], Steven P. Gygi[b], and Alexander Varshavsky[a,1]

[a]Division of Biology and Biological Engineering, California Institute of Technology, Pasadena, CA 91125; and [b]Department of Cell Biology, Harvard Medical School, Boston, MA 02115

Contributed by Alexander Varshavsky, October 15, 2020 (sent for review September 25, 2020; reviewed by Thomas Arnesen and William P. Tansey)

The Arg/N-degron pathway targets proteins for degradation by recognizing their N-terminal or internal degrons. Our previous work produced double-knockout (2-KO) HEK293T human cell lines that lacked the functionally overlapping UBR1 and UBR2 E3 ubiquitin ligases of the Arg/N-degron pathway. Here, we studied these cells in conjunction with RNA-sequencing, mass spectrometry (MS), and split-ubiquitin binding assays. 1) Some mRNAs, such as those encoding lactate transporter MCT2 and β-adrenergic receptor ADRB2, are strongly (∼20-fold) up-regulated in 2-KO cells, whereas other mRNAs, including those encoding MAGEA6 (a regulator of ubiquitin ligases) and LCP1 (an actin-binding protein), are completely repressed in 2-KO cells, in contrast to wild-type cells. 2) Glucocorticoid receptor (GR), an immunity-modulating transcription factor (TF), is up-regulated in 2-KO cells and also physically binds to UBR1, strongly suggesting that GR is a physiological substrate of the Arg/N-degron pathway. 3) PREP1, another TF, was also found to bind to UBR1. 4) MS-based analyses identified ∼160 proteins whose levels were increased or decreased by more than 2-fold in 2-KO cells. For example, the homeodomain TF DACH1 and the neurofilament subunits NF-L (NFEL) and NF-M (NFEM) were expressed in wild-type cells but were virtually absent in 2-KO cells. 5) The disappearance of some proteins in 2-KO cells took place despite up-regulation of their mRNAs, strongly suggesting that the Arg/N-degron pathway can also modulate translation of specific mRNAs. In sum, this multifunctional proteolytic system has emerged as a regulator of mammalian gene expression, in part through conditional targeting of TFs that include ATF3, GR, and PREP1.

transcription | degradation | UBR1 | GR | PREP1

Regulated protein degradation protects cells from abnormal (e.g., misfolded or aggregated) proteins and also modulates the levels of proteins that evolved to be short-lived in vivo. The bulk of intracellular protein degradation is mediated by the ubiquitin (Ub)-proteasome system (UPS) and by the autophagosome-endosome-lysosome system, with molecular chaperones playing essential roles in both processes (1–6). UPS comprises pathways that have in common two classes of enzymes, Ub ligases and deubiquitylases. An E3-E2 ligase recognizes a protein substrate through its feature called a degradation signal (degron) and conjugates a small protein Ub, usually in the form of a poly-Ub chain, to an amino acid residue of a substrate, usually its internal lysine. Deubiquitylases mediate, in particular, deubiquitylation of Ub-conjugated proteins (1–7). The 26S proteasome is a multisubunit ATP-dependent protease that binds to a poly-Ub of a ubiquitylated protein, unfolds the protein, and cleaves it to peptides that range from ∼3 to ∼25 residues (8–10).

N-degron pathways (they were previously called "N-end rule pathways") are proteolytic systems that can recognize proteins containing N-terminal (Nt) degrons called N-degrons. The targeted proteins are destroyed by the 26S proteasome and/or autophagy pathways in eukaryotes, and by the ClpS-ClpAP protease in bacteria (Fig. 1 and *SI Appendix*, Fig. S1) (2, 11–32). Specific determinants of an N-degron include a destabilizing Nt-residue of a protein, its internal lysine (or lysines) that functions as a site of polyubiquitylation, and a segment used by the proteasome to initiate degradation (2, 12).

The currently known eukaryotic N-degron pathways comprise the Arg/N-degron pathway (it targets, in particular, specific unacetylated Nt-residues); the Ac/N-degron pathway (it targets, in particular, the N^{α}-terminally acetylated [Nt-acetylated] Nt residues); the Pro/N-degron pathway (it targets, in particular, the Nt-Pro residue); the Gly/N-degron pathway (it targets the unmodified Nt-Gly residue); and the fMet/N-degron pathway (it targets Nt-formylated proteins) (Fig. 1 and *SI Appendix*, Fig. S1) (2, 11–28, 30–34).

Initially, most N-degrons are not active (pro-N-degrons). Active N-degrons are produced either constitutively (for example, cotranslationally) or via regulated steps. Many nonprocessive intracellular proteases, including aminopeptidases, caspases, calpains, separases, and cathepsins, function as "upstream" components of N-degron pathways that generate active N-degrons, since a cleavage of a protein can produce a C-terminal (Ct) fragment bearing a destabilizing Nt-residue (2, 23, 30). N-degrons can also be formed (activated) through enzymatic Nt-acetylation, Nt-deamidation, Nt-oxidation, Nt-arginylation, Nt-leucylation, and Nt-formylation of specific proteins or their Ct-fragments (Fig. 1 and *SI Appendix*, Fig. S1) (2, 16, 17, 19, 28). Recognition components of N-degron pathways are called N-recognins. They are E3 Ub ligases or other proteins (for example, mammalian p62 or bacterial ClpS) that can recognize N-degrons (2, 16, 25, 27, 29). In cognate sequence contexts, all 20 amino acids of the genetic code can act as destabilizing Nt-residues (*SI Appendix*, Fig. S1). Consequently, many proteins in a cell are conditionally short-lived substrates of N-degron pathways, either as full-length proteins or as Ct-fragments. An additional and functionally important feature

Significance

The Arg/N-degron pathway targets proteins for degradation by recognizing their N-terminal or internal degradation signals. In the present study, we compared wild-type human cells to their double-knockout (2-KO) counterparts that lacked the UBR1/UBR2 ubiquitin ligases of the Arg/N-degron pathway. We found that a number of specific genes were either strongly induced or strongly repressed in 2-KO cells. In addition, specific transcription factors, including glucocorticoid receptor, were identified here as physiological substrates of the Arg/N-degron pathway. We discuss the emerged role of this proteolytic system as a regulator of mammalian gene expression.

Author contributions: T.T.M.V., D.C.M., S.P.G., and A.V. designed research; T.T.M.V. and D.C.M. performed research; T.T.M.V., D.C.M., S.P.G., and A.V. analyzed data; and T.T.M.V., D.C.M., S.P.G., and A.V. wrote the paper.

Reviewers: T.A., University of Bergen; and W.P.T., Vanderbilt University.

The authors declare no competing interest.

[1]To whom correspondence may be addressed. Email: avarsh@caltech.edu.

This article contains supporting information online at https://www.pnas.org/lookup/suppl/doi:10.1073/pnas.2020124117/-/DCSupplemental.

First published November 23, 2020.

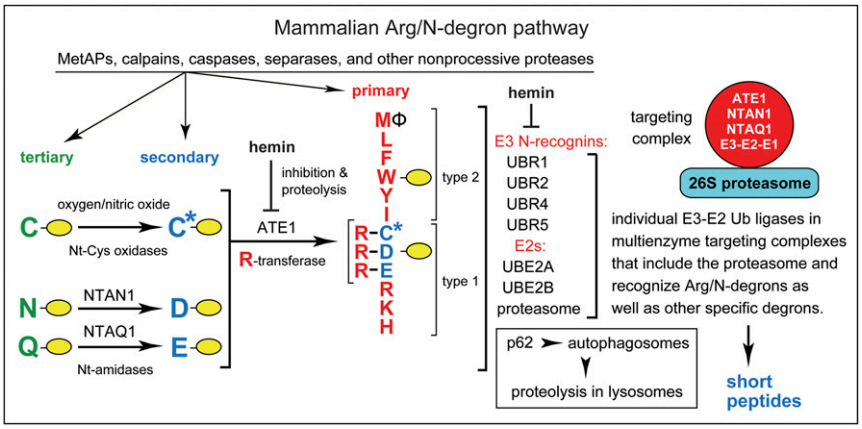

Fig. 1. The mammalian Arg/N-degron pathway (2, 15, 16). Single-letter abbreviations denote Nt-residues. The rest of a protein substrate is denoted by a yellow oval. The Arg/N-degron pathway targets proteins for degradation either by the 26S proteasome (via UBR1, UBR2, UBR4, and UBR5 E3s) or by the autophagy-lysosome pathway (via p62 N-recognin). The E3s cited above can recognize not only the indicated (primary destabilizing) Nt-residues of protein substrates but also specific non-N-terminal degrons in proteins that lack Arg/N-degrons. The terms "primary," "secondary," and "tertiary" denote specific classes of destabilizing Nt-residues. The Nt-amidases NTAN1 and NTAQ1 convert, respectively, Nt-Asn and Nt-Gln to the Nt-residues Asp and Glu. C* denotes an oxidized N-terminal Cys residue, either Cys-sulfinate or Cys-sulfonate. These derivatives of Nt-Cys can be produced in vivo through reactions that involve oxygen and NO. The Arg-tRNA-protein transferase (R-transferase) ATE1 conjugates Arg (with Arg-tRNA as a cosubstrate) to the Nt-Asp, Nt-Glu, or (oxidized) Nt-Cys residues. Hemin (Fe^{3+}-heme) down-regulates both the activity of R-transferase and its in vivo stability. Hemin also interacts with UBR1/UBR2. The terms "type 1" and "type 2" denote, respectively, the basic (Arg, Lys, and His) and bulky hydrophobic residues (Leu, Phe, Trp, Tyr, Ile, and also Met, if the latter is followed by a bulky hydrophobic residue [Φ]). Type 1 and type 2 primary destabilizing Nt residues are recognized by distinct substrate-binding sites of the pathway's E3 N-recognins. The UBR1 and UBR2 E3 Ub ligases are sequelogous to each other and to *S. cerevisiae* UBR1. Specific components of the human Arg/N-degron pathway have been shown to form a targeting complex (34). The *S. cerevisiae* Arg/N-degron pathway is also mediated by an analogous multienzyme complex (34). A "generic" targeting complex of the mammalian Arg/N-degron pathway (red circle on the *Right*) denotes a hypothetical set of analogous complexes. Only one of these complexes (containing UBR1 or UBR2 E3) was identified so far (34). Other, analogous targeting complexes may contain, in particular, either UBR4 or UBR5 E3s. A targeting complex is likely to include the 26S proteasome as well (34). The Ub-activating (E1) enzyme is expected to be a transient component of the complex, since E1 is a ligand of E2 enzyme. See Introduction for additional references.

of most E3 N-recognins is that they can target, through their multiple binding sites, not only N-degrons but other degradation signals as well. This ability of N-recognin E3s further expands the range of substrates targeted by N-degron pathways (Fig. 1) (2, 26, 35, 36).

Regulated degradation of proteins and their natural fragments by N-degron pathways has been shown to mediate a remarkably broad range of biological processes, including the sensing of oxygen, nitric oxide (NO), heme, and short peptides; the elimination of misfolded proteins and of proteins retrotranslocated to the cytosol from other compartments; the control of subunit stoichiometries in protein complexes; a suppression of neurodegeneration and regulation of apoptosis; the control of DNA repair, transcription, replication, and chromosome cohesion/segregation; the regulation of chaperones, cytoskeletal proteins, G proteins, autophagy, gluconeogenesis, peptide transport, meiosis, circadian rhythms, cell migration, fat metabolism, adaptive and innate immunity, the cardiovascular system, neurogenesis and spermatogenesis; and also plant defenses against pathogens, plant cell differentiation, the sensing of oxygen and NO, and many other processes in plants (2, 11–38 and refs. therein).

To keep notations uniform, human (*Homo sapiens*, *hs*) genetic terms (all-uppercase letters) are used below to denote both human, mouse (*Mus musculus*, *mm*) and yeast (*Saccharomyces cerevisiae*, *sc*) genes and proteins. *scUBR1* encodes the 225-kDa RING-type E3, the sole N-recognin of the *S. cerevisiae* Arg/N-degron pathway. Unmodified N-terminal Arg, Lys, His, Leu, Phe, Tyr, Trp, Ile, and Met (if Nt-Met is followed by a bulky hydrophobic residue) are termed "primary" destabilizing Nt-residues in that they can be bound by the type-1 and type-2 sites of *sc*UBR1 (2, 15, 16). In contrast, Nt-Asp and Nt-Glu are destabilizing, owing to their Nt-arginylation by *sc*ATE1 arginyltransferase (R-transferase). The Nt-conjugated Arg can be recognized by *sc*UBR1. Nt-Asn and Nt-Gln are destabilizing because *sc*NTA1 Nt-amidase can convert them to Nt-arginylatable, Nt-Asp and Nt-Glu (*SI Appendix*, Fig. S1*G*) (2, 32).

In contrast to *S. cerevisiae*, the mammalian Arg/N-degron pathway is mediated by at least four E3 N-recognins: the 200-kDa UBR1 and UBR2; the 570-kDa UBR4 (p600, BIG); and the 300-kDa UBR5 (EDD1, HYD) (Fig. 1) (2, 16, 25). Another, non-E3 N-recognin of this pathway is p62, an autophagy-regulating protein (27). *hs*UBR1 and *hs*UBR2 E3s are sequelogous[†] [similar in sequence (39)] to each other and to *S. cerevisiae* *sc*UBR1. In contrast, sequelogies (39) (sequence similarities) between *hs*UBR1/*hs*UBR2 and *hs*UBR4 or *hs*UBR5 are confined largely to their ∼80-residue folded UBR domains, which bind to N-terminal Arg, Lys, or His (2, 16). In *S. cerevisiae*, *sc*NTA1, an Asn/Gln/Nt-amidase, can deamidate either Nt-Asn or Nt-Gln, whereas animals and plants contain two Nt-amidases, the Nt-Asn-specific NTAN1 and Nt-Gln-specific NTAQ1 (Fig. 1 and *SI Appendix*, Fig. S1*G*) (2, 16).

In multicellular eukaryotes, Nt-arginylation encompasses not only Nt-Asp and Nt-Glu but also Nt-Cys, after its oxygen/NO-dependent oxidation to Nt-arginylatable Nt-Cys-sulfinate or

[†]"Sequelog" denotes a sequence that is similar, to a specified extent, to another sequence (39). Derivatives of sequelog include sequelogy (sequence similarity) and sequelogous (similar in sequence). The usefulness of sequelog and derivative notations stems from the rigor and clarity of their evolutionary neutrality. By contrast, in settings that use "homolog," "ortholog," and "paralog" (they denote, respectively, common descent and functional similarity/dissimilarity), these terms are often interpretation laden and imprecise. Homolog, ortholog, and paralog are compatible with the sequelog terminology. The former terms can be used to convey understanding about common descent and biological functions if this additional information, distinct from sequelogy per se, is actually present (39).

Nt-Cys-sulfonate (Fig. 1). As a result, the Arg/N-degron pathway functions as a sensor of oxygen/NO, through the conditional and arginylation-dependent degradation of Nt-Cys-bearing transcription factors and regulators of G proteins (13, 18, 28). Five enzymes of the human Arg/N-degron pathway (UBR1 or UBR2 E3, UBE2A or UBE2B E2, ATE1 R-transferase, NTAN1 Asn/Nt-amidase, and NTAQ1 Gln/Nt-amidase) form a targeting complex (34) (Fig. 1). An analogous multienzyme complex mediates the *S. cerevisiae* Arg/N-degron pathway (34).

Homozygous inactivation of human *hsUBR1* (with retention of other E3 Arg/N-recognins; Fig. 1) causes a birth defect called Johanson-Blizzard syndrome (JBS). Its symptoms include exocrine pancreatic insufficiency and inflammation, anatomical malformations, mental retardation, and deafness (2, 40). *mmUBR1*$^{-/-}$ mice have a milder version of JBS (40). Abnormal phenotypes of *mmUBR2*$^{-/-}$ mice include infertility of males, owing to apoptosis of *mmUBR2*$^{-/-}$ spermatocytes (2, 16). Mouse (or human) UBR1 and UBR2 E3s are 47% identical and overlap functionally (2, 15, 16). In contrast to viability of single-mutant *mmUBR1*$^{-/-}$ and *mmUBR2*$^{-/-}$ mouse strains, mice that lack both *mm*UBR1 and *mm*UBR2 die as midgestation embryos, with massive neural and cardiovascular defects (41).

Our previous work described construction of conditional double-knockout (2-KO) adult (*mmUBR1*$^{-/-}$ *mmUBR2*$^{-/-}$) mice and also unconditional 2-KO (*hsUBR1*$^{-/-}$ *hsUBR2*$^{-/-}$) human HEK293T cell lines that lacked both *hs*UBR1 and *hs*UBR2 (42). Employing these tools, we identified ATF3, a stress-inducible basic leucine zipper (bZIP) transcription factor (TF) that regulates hundreds of genes, as a short-lived substrate of the Arg/N-degron pathway (42).

In the present study, we used split-Ub protein-binding assays, RNA-sequencing (RNA-seq), and quantitative mass spectrometry (MS) (42–45) to search for other TFs that interact with *hs*UBR1/*hs*UBR2 and also to compare the levels of specific mRNAs and proteins between wild-type human HEK293T cells and their 2-KO (*hsUBR1*$^{-/-}$ *hsUBR2*$^{-/-}$) mutants. The results described here include identification of the glucocorticoid receptor (*hs*GR) TF and *hs*PREP1 TF as putative substrates of the Arg/N-degron pathway, in part because both TFs interact with *hs*UBR1. The levels of some mRNAs and proteins were found to strongly differ between 2-KO and wild-type human cells. For example, we observed ∼20-fold increases of specific mRNAs (and encoded proteins) in 2-KO cells or an essentially complete repression of other mRNAs (and encoded proteins) in 2-KO cells. For instance, a TF called DACH1 and the main neurofilament subunits NF-L and NF-M were robustly expressed in wild-type cells but were virtually absent in 2-KO cells. Tellingly, a disappearance or near disappearance of some proteins in 2-KO cells took place despite increases in the levels of their mRNAs, strongly suggesting that the UBR1/UBR2-mediated Arg/N-degron pathway can also modulate translation of specific mRNAs. In sum, this multifunctional proteolytic system has emerged as a regulator of mammalian gene expression, in part through conditional targeting of TFs that include ATF3, GR, and PREP1.

Results and Discussion

Human 2-KO (*hsUBR1*$^{-/-}$ *hsUBR2*$^{-/-}$) HEK293T cell lines that lacked both *hs*UBR1 and *hs*UBR2, two sequelogous (39) and functionally overlapping E3 N-recognins (Fig. 1), were constructed and characterized in our preceding study (42). We describe here the use of 2-KO cells and other tools to identify specific substrates and functions of this pathway.

RNA-Seq Analyses of Wild-Type Versus 2-KO (*hsUBR1*$^{-/-}$ *hsUBR2*$^{-/-}$) Human Cells. Genome-wide quantitative RNA-seq was carried out with RNA preparations from wild-type and 2-KO human HEK293T cells (Fig. 2 and *SI Appendix*, Figs. S2–S7). Our initial aim was to determine whether the ablation of *hs*UBR1/*hs*UBR2 would cause not only moderate alterations of gene expression but also significantly higher than twofold changes in the levels of specific human mRNAs. If large effects in either direction would be observed, we planned to verify them by independent methods. A focus on strong changes stemmed from the expectation that a major effect of ablating *hs*UBR1/*hs*UBR2 on the level of a specific mRNA would facilitate the understanding of a link between that effect and the Arg/N-degron pathway.

Relative mRNA levels were the averages of three independent RNA-seq measurements for wild-type and 2-KO HEK293T cell lines. The scatter of RNA-seq data among three datasets (for each of these cell lines), particularly for mRNAs whose levels changed by more than twofold in either direction, was quite low (<5%) (*SI Appendix*, Fig. S2). Some mRNAs analyzed by RNA-seq were also quantified by ^{32}P-Northern hybridization and/or RT-qPCR. The results were in at least qualitative agreement with RNA-seq data (Fig. 2 and *SI Appendix*, Figs. S2–S5). In these measurements, a second, independently constructed 2-KO HEK293T cell line, denoted as 2-KO #2, was also used as additional control (Fig. 2 *A*, *B*, and *E* and *SI Appendix*, Fig. S3).

RNA-seq analyses (Fig. 2 and *SI Appendix*, Figs. S2, S4–S7) quantified mRNA levels for ∼18,000 human genes. Among them, 161 (<1%) genes exhibited at least twofold increases of mRNAs in 2-KO cells. Conversely, 211 (<2%) genes were decreased by twofold or more (Fig. 2 and *SI Appendix*, Figs. S2 and S5 *A*–*C*). We confined further analyses to genes for which the maximal level of a specific mRNA, in either 2-KO or wild-type cells, comprised at least 50 sequence "reads." Each read is an alignment of a sequenced, RNA-seq-detected segment of mRNA to the reference human genome (*SI Appendix*, Figs. S6 and S7). Consequently, the above 161 genes up-regulated by twofold or higher became 39 genes, chosen for high-confidence (at least 50 sequence reads) increases of mRNA in 2-KO cells. Analogously, the above 211 down-regulated genes became 93 genes, selected for high-confidence twofold or stronger decreases of mRNA levels in 2-KO cells (Fig. 2 and *SI Appendix*, Figs. S2–S7).

The 132 (39 + 93) altered-level mRNAs, that were chosen using criteria described above for explicit citation, comprise a high-confidence subset of all mRNAs whose levels were altered, in either direction, between 2-KO and wild-type cells (Fig. 2 and *SI Appendix*, Figs. S2–S7). *SI Appendix*, Fig. S4 cites 39 human mRNAs whose levels were increased in 2-KO cells by at least 2-fold (from 22-fold to 2-fold). The fold values, measured by RNA-seq and also for some mRNAs by ^{32}P-Northerns and RT-qPCRs, are shown in black, red, and green, respectively (*SI Appendix*, Fig. S4). Descriptions of encoded proteins that are TFs or components of the Ub system are in red and blue, respectively (*SI Appendix*, Fig. S4). *SI Appendix*, Fig. S5 uses the same notations, citing 93 mRNAs that were decreased by at least 2-fold (from ∼100-fold to 2.0-fold).

Up-Regulation of Specific Human mRNAs in 2-KO Cells. In the above sets of mRNAs, our analyses concentrated on 10 up-regulated and 10 down-regulated mRNAs for which the effects of ablating *hs*UBR1/*hs*UBR2 were particularly strong (Fig. 2*D*). It should be emphasized that alterations in the levels of other mRNAs, the ones not cited in Fig. 2*D* (*SI Appendix*, Figs. S4 and S5), are also worth exploring further, since many of these changes are likely to be as significant functionally as the strongest effects.

In the 10-gene set of up-regulated mRNAs, two of them, *hsADRB2*, encoding β-adrenergic receptor-2, and *hsMCT2* (*hsSLC16A7*), encoding a monocarboxylate transporter, were increased by 17-fold and 22-fold, respectively (Fig. 2 *B* and *D* and *SI Appendix*, Fig. S4). In the former case, which was quantified independently by ^{32}P-Northerns, the detection of *hsADRB2* mRNA in wild-type cells required a strong overexposure of ^{32}P-autoradiograms (Fig. 2*B*, lanes 7 and 8; compare to lanes 4

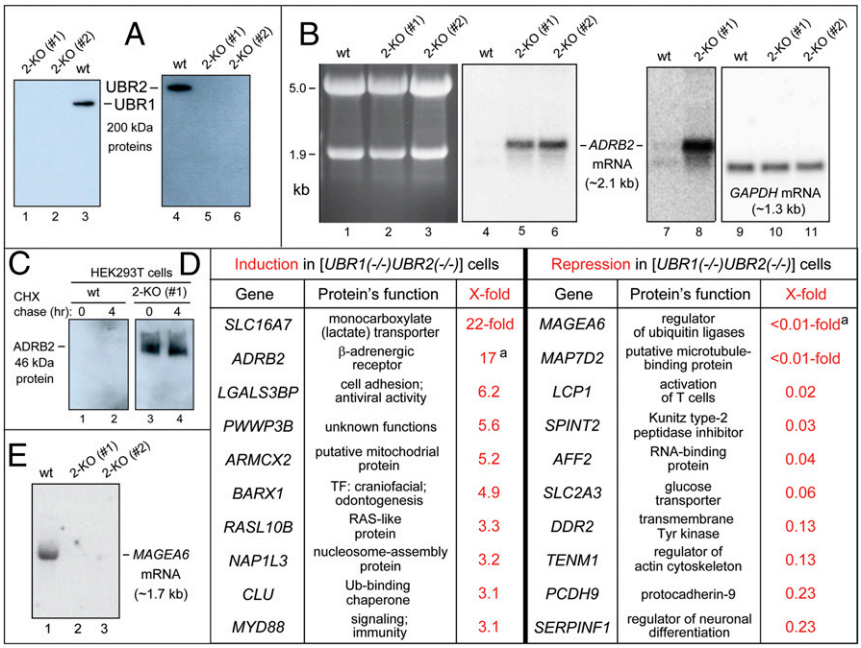

Induction in [*UBR1(-/-)UBR2(-/-)*] cells

Gene	Protein's function	X-fold
SLC16A7	monocarboxylate (lactate) transporter	22-fold
ADRB2	β-adrenergic receptor	17 [a]
LGALS3BP	cell adhesion; antiviral activity	6.2
PWWP3B	unknown functions	5.6
ARMCX2	putative mitochodrial protein	5.2
BARX1	TF: craniofacial; odontogenesis	4.9
RASL10B	RAS-like protein	3.3
NAP1L3	nucleosome-assembly protein	3.2
CLU	Ub-binding chaperone	3.1
MYD88	signaling; immunity	3.1

Repression in [*UBR1(-/-)UBR2(-/-)*] cells

Gene	Protein's function	X-fold
MAGEA6	regulator of ubiquitin ligases	<0.01-fold [a]
MAP7D2	putative microtubule-binding protein	<0.01-fold
LCP1	activation of T cells	0.02
SPINT2	Kunitz type-2 peptidase inhibitor	0.03
AFF2	RNA-binding protein	0.04
SLC2A3	glucose transporter	0.06
DDR2	transmembrane Tyr kinase	0.13
TENM1	regulator of actin cytoskeleton	0.13
PCDH9	protocadherin-9	0.23
SERPINF1	regulator of neuronal differentiation	0.23

Fig. 2. Summary of RNA-seq and related analyses of wild-type (wt) vs. 2-KO (*hsUBR1*$^{-/-}$ *hsUBR2*$^{-/-}$) human HEK293T cells. (*A*) IB analyses of the wild-type (parental) HEK293T cell line and two independently produced 2-KO cell lines, #1 and #2, using anti-*hs*UBR1 and anti-*hs*UBR2 antibodies. (*B*) Lanes 1 through 3, fractionated total RNA, stained with ethidium bromide, from wild-type HEK293T cells and 2-KO cell lines #1 and #2. The bands of 18S and 28S rRNAs are indicated on the *Left*. Lanes 4 through 6, Northern hybridization, using a ^{32}P-labeled RNA probe specific for the ~2.1-kb *hsADRB2* mRNA, of blotted RNAs in lanes 1 through 3. Lanes 7 and 8, same as lanes 4 and 5, but a 7-fold longer autoradiographic exposure to detect *hsADRB2* mRNA in wild-type cells (lane 7). Lanes 9 through 11, same as lanes 4 through 6, but hybridization with a ^{32}P-labeled RNA probe specific for the ~1.3-kb *hsGAPDH* mRNA (loading control). (*C*) Lanes 1 and 2, IB-based (using anti-*hs*ADRB2 antibody) CHX chase, for 0 and 4 h, of *hs*ADRB2 in wild-type HEK293T cells. Lanes 3 and 4, same as lanes 1 and 2, but with 2-KO cell line #1, in which *hsADRB2* mRNA was up-regulated by 17-fold (see *B* and the main text). (*D*) The list of 10 human mRNAs that were up-regulated by at least 3.1-fold (from 22-fold to 3.1-fold) in 2-KO cell line #1, and the analogous list of 10 mRNAs that were down-regulated by at least 4.3-fold (from more than 100-fold to 4.3-fold) in the above 2-KO cells. Superscript "a" in the right column denotes a minimal estimate of the extent of observed repression. (*E*) ^{32}P-Northern analysis (see *B*) of the repression of *hsMAGE6* mRNA (see *D*) in 2-KO cell lines #1 and #2 (lanes 2 and 3) vs. robust expression of *hsMAGE6* in wild-type cells (lane 1).

and 5). Four mRNAs, encoding *hs*LGALS3BP (it functions in cell adhesion), *hs*PWWP3B (a protein of unknown function), *hs*ARMCX2 (a putative mitochondrial protein), and *hs*BARX1 (a TF that mediates craniofacial development and odontogenesis), were increased, in 2-KO cells, by 6.2-fold, 5.6-fold, 5.2-fold, and 4.9-fold, respectively (Fig. 2*D* and *SI Appendix*, Figs. S3*A* and S4).

In the 10-gene set of down-regulated mRNAs, 3 of them encoding *hs*MAGEA6 (a regulator of Ub ligases), *hs*MAP7D2 (a putative microtubule-binding protein), and *hs*LCP1 (an actin-binding protein), were decreased by at least 50-fold, from robust expression in wild-type cells to undetectable or nearly undetectable levels in 2-KO cells (Fig. 2 *D* and *E* and *SI Appendix*, Fig. S5*A*). mRNAs encoding *hs*SPINT2 (a peptidase inhibitor), *hs*AFF2 (an RNA-binding protein), and *hs*SLC2A3 (a glucose transporter) were decreased, in 2-KO cells, by 33-fold, 25-fold, and 16-fold, respectively (Fig. 2*D* and *SI Appendix*, Figs. S5*A* and S7).

***hsADRB2* mRNA, Encoding β-Adrenergic Receptor-2, Is Increased by 17-Fold in 2-KO Cells.** The mammalian ADRB2 β-adrenergic receptor-2, a multispanning transmembrane protein, is expressed in most tissues. ADRB2 recognizes catecholamines (including epinephrine), is coupled to a subset of G proteins and regulates in particular the levels of cyclo-AMP (cAMP) (46–48). The 17-fold up-regulation of *hsADRB2* mRNA in 2-KO cells was accompanied by a robust expression of *hs*ADRB2 protein in these cells, as indicated by immunoblotting (IB) with antibody to *hs*ADRB2 (Fig. 2 *B–D* and *SI Appendix*, Fig. S4). In contrast, *hs*ADRB2 was undetectable by IB in wild-type cells, in agreement with near-zero levels of *hsADRB2* mRNA in those cells (Fig. 2*B*).

Comparisons of Transcriptional Promoters to Address Overexpression of *hsADRB2* in 2-KO Cells. The *hsADRB1* gene, encoding β-adrenergic receptor-1, was not up-regulated in 2-KO (*hsUBR1*$^{-/-}$ *hsUBR2*$^{-/-}$) HEK293T cells, in contrast to *hsADRB2*, which encodes a protein highly sequelogous to *hs*ADRB1 (Fig. 2 *B–D* and *SI Appendix*, Figs. S3 and S4). (Levels of *hsADRB1* mRNA were too low for detection by RNA-seq in both 2-KO and wild-type cells.) While the 17-fold increase of *hsADRB2* mRNA in 2-KO cells (Fig. 2*D* and *SI Appendix*, Fig. S4) might result in part from a metabolic stabilization of this mRNA, a parsimonious interpretation is that at least the bulk of this increase is caused by transcriptional induction of *hsADRB2* in the absence of *hs*UBR1/*hs*UBR2.

For reasons that include large DNA spans and complexity of mammalian transcriptional control, our comparisons of *hsADRB2* and *hsADRB1* promoters were confined to ~2-kb DNA segments upstream of transcription start sites. Our aim was to identify experimentally tractable differences in the patterns of specific TF-binding sites between these promoters, with the possibility of expanding, later, a search for differences beyond initially examined DNA segments (*SI Appendix*, Fig. S8). *hsADRB1* and *hsADRB2* have been previously mapped using expression assays, mutagenesis, gel-shift DNA binding, and other methods (47, 48). *hsADRB1* and *hsADRB2* promoters contain binding sites for a number of TFs, including *hs*NF-κB, *hs*AP2,

and *hs*SP1. Most of these and other TF-binding sites are shared between *hsADRB1* and *hsADRB2*. Nevertheless, we detected two possible (nonalternative) causes of "up-regulation" difference between these otherwise similar genes.

First, *hsADRB2* promoter contains two sites that can bind to *hs*SP1, an activator TF that up-regulates many genes (*SI Appendix*, Fig. S8) (49). In contrast, the analogous region of *hsADRB1* contains one *hs*SP1-binding site (*SI Appendix*, Fig. S8). Second, the single *hs*SP1-binding site in *hsADRB1* overlaps with a site recognized by *hs*EGR1, a transcriptional repressor (47, 48). Thus, interactions of *hs*SP1 and *hs*EGR1 TFs with *hsADRB1* promoter are likely to be mutually exclusive (*SI Appendix*, Fig. S8). Significantly, the *hsADRB2* promoter lacks a binding site for the *hs*EGR1 repressor, in contrast to *hsADRB1*. Finally, the *hs*EGR1 repressor may be, at least in part, a substrate of the Arg/N-degron pathway; this remains to be verified. If so, *hs*EGR1 would be up-regulated in 2-KO cells and would act to inhibit transcription of *hsADRB1*, but not of *hsADRB2*. This mechanistically specific and testable model (*SI Appendix*, Fig. S8) is ready to be verified in future experiments.

hsMCT2 mRNA, Encoding a Monocarboxylate Transporter, Is Increased by 22-Fold in 2-KO Cells. *hs*MCT2 (*hs*SLC16A7) is a proton-linked transporter of monocarboxylates such as lactate, pyruvate, and ketone bodies (50, 51). *hsMCT2* mRNA was increased by 22-fold in 2-KO cells, as discovered by RNA-seq and confirmed by RT-qPCR (the latter method suggested an even higher, 35-fold increase of *hsMCT2* mRNA in 2-KO cells) (Fig. 2*D* and *SI Appendix*, Fig. S4). The family of mammalian SLC16 (MCT) transporters comprises 14 proteins. Substrates and partial functions are known for only seven of these transporters (50, 51). Mammalian MCT2 is expressed in most tissues and can mediate either influx or efflux of its substrates, depending on substrate levels and a pH gradient across a membrane (either the plasma membrane or specific intracellular membranes). Functions of MCT2 include lactate transport, particularly in the brain and skeletal muscle (50).

In contrast to *hsMCT2* mRNA, which was increased by 22-fold in 2-KO cells (Fig. 2*D* and *SI Appendix*, Fig. S4), RNA-seq did not detect mRNAs of 11 *hsSLC16*-family genes in either wild-type or 2-KO cells. Two *hsSLC16* family members other than *hsMCT2*, specifically *hsMCT1* (*hsSLC16A7*) and *hsMCT8* (*hsSLC16A2*) mRNAs, were increased by 1.1-fold and 1.4-fold, respectively, in 2-KO cells. Furthermore, MS-based protein analyses (see below) of 2-KO cell lines #1 and #2 vs. wild-type cells indicated, respectively, 2.4-fold and 4-fold decreases of the *hs*MCT8 protein in 2-KO cells (*SI Appendix*, Fig. S12*B*), a direction of changes that is opposite to 22-fold induction of *hsMCT2* mRNA (Fig. 2*D*) and up-regulation of *hs*MCT2 protein (see below).

The selective and massive up-regulation of *hsMCT2* mRNA upon the ablation of *hs*UBR1/*hs*UBR2 (Fig. 2*D* and *SI Appendix*, Fig. S4) opens up the same strategy of comparing transcriptional promoters that yielded a verifiable model of selective up-regulation of the *hsADRB2* gene in 2-KO cells (*SI Appendix*, Fig. S8). Analogous promoter comparisons are also possible with other genes that are up-regulated or down-regulated in 2-KO cells (Fig. 2*D*). In the present paper, such comparisons are confined to *hsADRB2* vs. *hsADRB1* (*SI Appendix*, Fig. S8), inasmuch as verifications of resulting models are still in the future.

Double-KO HEK293T Cells, Which Overexpress _hsMCT2_ mRNA, Are Hypersensitive to Dimethyloxalylglycine. MS-based protein analyses (see below) confirmed an up-regulation of *hs*MCT2 protein in 2-KO cells, with, respectively, 6.0-fold and 2.7-fold increases of *hs*MCT2 in 2-KO cell lines #1 and #2 (*SI Appendix*, Fig. S12*A*).

To address this question in a different way, we asked whether the 22-fold increase of *hsMCT2* mRNA in 2-KO cells (Fig. 2*D* and *SI Appendix*, Fig. S4) and the resulting increase of encoded protein cause a phenotype that can be traced to the level of *hs*MCT2. The metabolite α-ketoglutarate (αKG) is a cosubstrate (together with oxygen) of αKG-dependent dioxygenases (αKGDDs), a family of enzymes that include prolyl hydroxylases (PHDs). The oxygen-dependent hydroxylation by PHDs of specific Pro residues in, for example, HIFα TF (which mediates responses to oxygen), activates its degron and thereby regulates, through oxygen-modulated degradation of HIFα, the expression of genes controlled by HIFα (52, 53).

N-oxalylglycine (NOG), a synthetic analog of αKG, is a cytotoxic inhibitor of αKGDD enzymes, but NOG cannot enter cells (51). Dimethyloxalylglycine (DMOG), a derivative of NOG, is rapidly hydrolyzed in aqueous solutions to methyloxalylglycine (MOG). Upon its entry into cells, MOG is converted to NOG. The import of MOG is mediated largely by the MCT2 transporter (51). Consequently, an up-regulation of *hs*MCT2 in 2-KO cells would predict their hypersensitivity to extracellular DMOG, in comparison to wild-type cells.

To compare sensitivities of cells to DMOG, we used a cell mass accumulation assay (51). In the absence of DMOG, 2-KO cell cultures grew at rates similar to those of parental HEK293T cells (*SI Appendix*, Fig. S9*A*). In contrast, proliferation of 2-KO cells was found to be at least 5.4-fold more sensitive to DMOG than proliferation of wild-type cells (*SI Appendix*, Fig. S9*B*). "At least" refers to the fact that parameters of the cell accumulation assay were not varied to maximize the measured difference in sensitivity to DMOG between two cell lines.

These results (*SI Appendix*, Fig. S9), together with previous demonstration that *hs*MCT2 is the main MOG importer (51), confirm the above prediction that 2-KO cells, which overexpress both *hsMCT2* mRNA and the encoded protein (Fig. 2*D* and *SI Appendix*, Figs. S4 and S11*A*), would be hypersensitive to growth suppression by DMOG (specifically by NOG, which DMOG is converted to, via MOG).

Other Genes That Are Up-Regulated in 2-KO Cells. In addition to *hsADRB2* and *hsMCT2* mRNAs (increased by 17-fold and 22-fold, respectively), several other mRNAs (*hsLGALS3BP*, *hsPWWP3B*, *hsARMCX2*, and *hsBARX1*) were also up-regulated by more than 4-fold in 2-KO cells (Fig. 2*D* and *SI Appendix*, Fig. S4). *hs*LGALS3BP is a protein that promotes cell adhesion (https://www.uniprot.org/uniprot/Q08380). *hs*PWWP3B is a broadly expressed protein of unknown function (https://www.uniprot.org/uniprot/Q5H9M0) (Fig. 2*D* and *SI Appendix*, Fig. S4). *hs*ARMCX2 is a largely uncharacterized protein (https://www.uniprot.org/uniprot/Q7L311) (Fig. 2*D* and *SI Appendix*, Fig. S4). *hs*BARX1 is a homeodomain TF that is important for development of craniofacial bones, teeth, cartilage, muscle, spleen, stomach, and esophagus (54). The increase of *hsBARX1* mRNA in 2-KO HEK293T cells (4.9-fold by RNA-seq; 7.3-fold by RT-qPCR) (Fig. 2*D* and *SI Appendix*, Figs. S3*A* and S4) may be caused by a decreased degradation, in the absence of *hs*UBR1/*hs*UBR2, of an unknown activator TF whose stabilization accelerates transcription of *hsBARX1*. A nonalternative possibility is that *hs*BARX1 TF is a positive regulator of its own gene and a short-lived substrate of the Arg/N-degron pathway.

Repression of Specific Genes in 2-KO Cells. *hsMAGEA6* is a member of the family of human *MAGE* genes. Some MAGE proteins, including *hs*MAGEA6, are components and modulators of specific Ub ligases. *MAGE* genes, including *hsMAGEA6*, are often ectopically expressed in cancer cells, in which specific MAGEs can act as oncogenic drivers (55). We found that *hsMAGEA6* mRNA was expressed in wild-type cells, but was decreased by at least 100-fold, i.e., was in effect shut off in 2-KO cells (Fig. 2 *D*

and *E* and *SI Appendix*, Fig. S5*A*). *hsLCP1* mRNA, which encodes an actin-binding protein (https://www.uniprot.org/uniprot/P13796), was decreased, in 2-KO cells by at least 50-fold to <2% of its level in wild-type cells (Fig. 2*D* and *SI Appendix*, Fig. S5*A*). *hsSLC2A3* mRNA, which encodes a glucose transporter (https://www.uniprot.org/uniprot/P11169), was decreased in 2-KO cells to <6% of its level in wild-type cells (Fig. 2*D* and *SI Appendix*, Fig. S5*A*).

Mass Spectrometric Analyses of Proteins in Wild-Type and 2-KO HEK293T Cells. MS-based protein surveys employed the quantitative TMT-SPS-MS3 (targeted mass tags-based sample multiplexing-mass spectrometric-3) technique (45) and were carried out with protein preparations from wild-type vs. 2-KO HEK293T cells (*SI Appendix*, Fig. S10). The TMT-SPS-MS3 method is summarized in *SI Appendix*, Fig. S11. TMT-SPS-MS3 analyses of wild-type and two 2-KO cell lines (#1 and #2) encompassed 83,513 peptides and corresponded to 7,714 different human proteins. Cited below are the main MS-based results:

1) A total of 45 proteins were found to be up-regulated, relative to wild-type HEK293T cells, by at least 2-fold in the 2-KO #1 cell line. In most (though not all) cases, these proteins were also classed as up-regulated in the 2-KO cell line #2 (*SI Appendix*, Fig. S12 *A* and *B*).
2) A total of 111 proteins were found to be down-regulated relative to wild-type cells by at least 2-fold in 2-KO cells (Fig. 3 and *SI Appendix*, Fig. S13 *A–D*).
3) The above proteins (156 = 45 + 111), whose levels were significantly increased or decreased in 2-KO HEK293T cells, relative to wild-type cells, encompassed a vast range of functions or putative functions (*SI Appendix*, Figs. S12 *A* and *B* and S13 *A–D*).
4) Changes in levels of the above 156 proteins (156 = 45 + 111) in 2-KO cells, as determined by MS analyses, will be gradually verified in future studies by independent methods, including quantitative IB. Verifications were initiated here with three proteins, *hs*DACH1, *hs*NF-L (*hs*NFEL), and *hs*NF-M (*hs*NFEM). According to MS, these proteins were down-regulated, respectively, by ∼5-fold, ∼16-fold, and ∼16-fold, in 2-KO cells, relative to wild-type cells (*SI Appendix*, Fig. S13*A*).

Using IB, we confirmed these findings (Fig. 3). Moreover, IB analyses showed that these endogenous, untagged proteins, while robustly expressed in wild-type HEK293T cells, either disappeared or nearly disappeared in 2-KO cell lines #1 and #2 (Fig. 3). Thus, the extents of repression of these three proteins in 2-KO cells that were measured by quantitative IB were even greater than MS-suggested repression levels (Fig. 3 and *SI Appendix*, Fig. S13*A*; see also below). These findings suggest that MS analyses, while invaluable for discovering specific proteins that are down-regulated in 2-KO cells (*SI Appendix*, Fig. S13 *A–D*), may underestimate the extents of their repression. This circumstance encourages future analyses of MS-identified proteins that are down-regulated in 2-KO cells (*SI Appendix*, Fig. S12 *A–D*) using independent methods, including quantitative IB. Described below are our first IB results with *hs*DACH1, *hs*NF-L, and *hs*NF-M.

Near Disappearance of the *hs*DACH1 Transcription Factor in 2-KO Cells. The 758-residue *hs*DACH1 is a TF whose functions include tumor suppression and regulation of organogenesis (56). According to TMT-SPS-MS3 data, the levels of *hs*DACH1 protein in 2-KO cells, in comparison to wild-type cells, were decreased by ∼5-fold and ∼3-fold, respectively, in 2-KO cell lines #1 and #2 (*SI Appendix*, Fig. S13*A*).

IB analyses of endogenous, untagged *hs*DACH1 using anti-*hs*DACH1 antibody and chemiluminescence-based IB showed a robust expression of *hs*DACH1 in wild-type HEK293T cells and an even stronger (more than 10-fold) repression of the *hs*DACH1 protein in 2-KO #1 and #2 cell lines than the extent of down-regulation estimated by MS (Fig. 3*A* and *SI Appendix*, Fig. S13*A*). Detection of proteins by IB using chemiluminescence is more sensitive than quantitative detection using near-infrared fluorescence dyes and an Odyssey-type scanner, but the former method is at best semiquantitative, hence the above minimal estimate rather than a measurement. With a near-infrared quantitative system, detection of *hs*DACH1 in 2-KO cells would have been impossible without a strong sample overload. Possible causes of the near disappearance of *hs*DACH1 in 2-KO cells (Fig. 3*A*) are mentioned below.

Near Disappearance of the Neurofilament Subunits NF-M and NF-L in 2-KO Cells. Neurofilaments are a specific class of intracellular intermediate filaments. Four main subunits of mammalian neurofilaments are NF-L (encoded by *NFEL*), NF-M (encoded by *NFEM*), NF-H (encoded by *NFEH*), and either α-internexin (encoded by *INA*) or peripherin (encoded by *PRPH*) (57, 58). Neurofilaments are present largely in neurons. Most HEK293T (and related) cell lines (which were produced by transformation of primary cultures of human embryonic kidney [HEK] cells with fragments of adenoviral DNA) contain neurofilaments and express their subunits, suggesting that HEK cell lines are actually of neuronal origin (59). Our wild-type HEK293T cells contained at least the NF-L, NF-M, and α-internexin subunits (Fig. 3*B*, lanes 1 and 2; Fig. 3 *C* and *E*, lanes 1 and 4, and *SI Appendix*, Figs. S12*A* and S13*A*).

In neurons, neurofilaments are present in both perikarya and dendrites and are particularly abundant in axons, in which they play major roles. Neurofilaments are regulated by phosphorylation and other modifications, and interact with a number of intracellular proteins. Abnormal accumulations of neurofilaments are characteristic of many diseases, including amyotrophic lateral sclerosis, Charcot-Marie-Tooth disease, neurofilament inclusion disease, giant axonal neuropathy, spinal muscular atrophy, and both Alzheimer's and Parkinson's diseases. Aberrant overproduction of neurofilaments in these diseases apparently contributes in major ways to the death of affected neurons (57, 58).

According to MS, the levels of *hs*NF-M protein were decreased by ∼16-fold in both 2-KO cell lines, #1 and #2, relative to wild-type cells (*SI Appendix*, Fig. S13*A*). IB analyses (using anti-*hs*NF-M antibody) confirmed these results. Moreover, the endogenous, untagged *hs*NF-M protein, while robustly expressed in wild-type HEK293T cells, was nearly undetectable by IB in both 2-KO cell lines, suggesting an even greater than ∼16-fold repression of *hs*NF-M in 2-KO cells (Fig. 3*B* and *SI Appendix*, Fig. S13*A*). Cycloheximide (CHX) chases of *hs*NF-M indicated its stability over 4 h in wild-type cells (Fig. 3*B*), in agreement with earlier findings (57, 58).

Similar results were obtained with *hs*NF-L, another neurofilament subunit, which binds to *hs*NF-M. According to MS, the level of *hs*NF-L was decreased, respectively, by ∼16-fold and ∼20-fold in 2-KO cell lines #1 and #2, relative to wild-type cells (*SI Appendix*, Fig. S13*A*). IB analyses of *hs*NF-L (using anti-*hs*NF-L antibody) employed both the quantitative Odyssey IB system and chemiluminescence-based IB. These and other IB assays also used antibody to glyceraldehyde 3-phosphate dehydrogenase (*hs*GAPDH) to detect *hs*GAPDH as a loading control (Fig. 3 *C–E*).

IBs detected expression of the endogenous, untagged *hs*NF-L protein in wild-type HEK293T cells and also indicated a complete or nearly complete disappearance of *hs*NF-L in both 2-KO cell lines (Fig. 3 *C–E*). Quantification using the Odyssey system of the repression of *hs*NF-L in 2-KO cells yielded an ∼40-fold

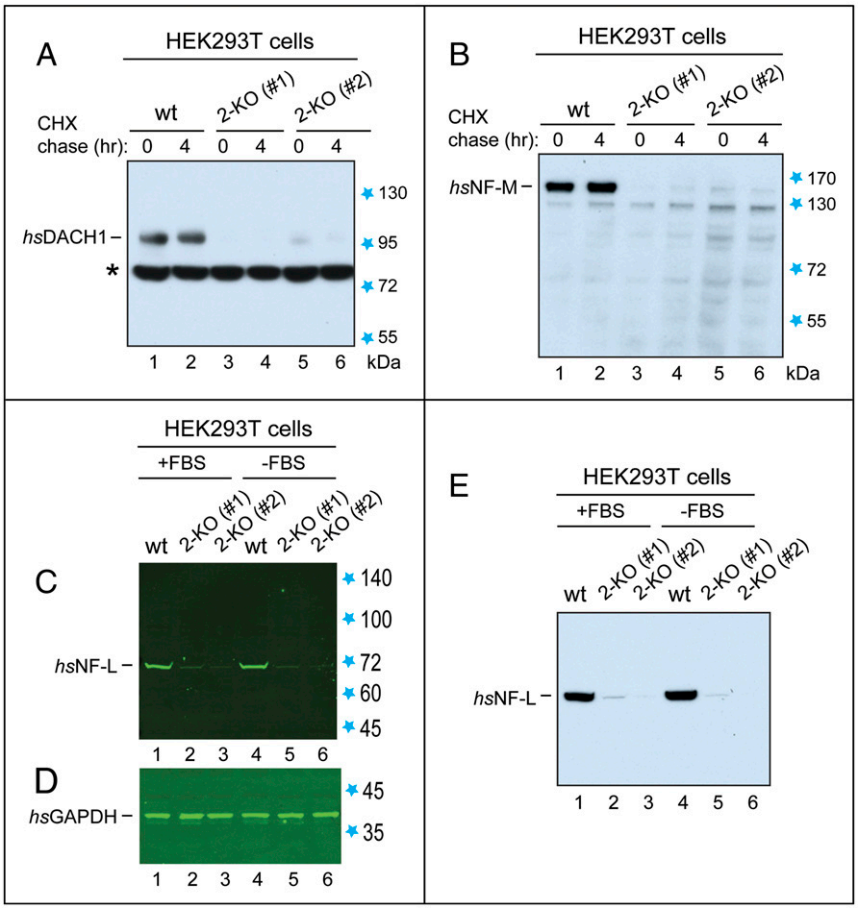

Fig. 3. Immunoblot analyses of proteins whose down-regulation in 2-KO (*hsUBR1*$^{-/-}$ *hsUBR2*$^{-/-}$) human HEK293T cells was initially detected by MS. Unless stated otherwise, cells were grown in the presence of fetal bovine serum (FBS). Detection of bound antibodies was performed using chemiluminescence (in *A*, *B*, and *E*) or near-infrared fluorescence and an Odyssey-type scanner (in *C* and *D*). (*A*) Lanes 1 and 2, IB-based CHX chase (using anti-*hs*DACH1 antibody) for 0 and 4 h of *hs*DACH1 TF in extracts from wild-type HEK293T cells. Lanes 3 and 4, same as lanes 1 and 2, but with 2-KO cell line #1. Lanes 5 and 6, same as in lanes 3 and 4, but with 2-KO cell line #2. Blue stars, in this and other panels, indicate positions of molecular mass markers. Black asterisk indicates a cross-reacting protein. (*B*) Same as in *A*, but with the *hs*NF-M subunit of neurofilaments, using anti-*hs*NF-M antibody. The apparent (anomalous) M_r (molecular mass), upon sodium dodecyl sulfate/polyacrylamide gel electrophoresis (SDS/PAGE), of the 916-residue *hs*NF-M is ∼150 kDa. (*C*) Lanes 1 through 3, IB analyses of *hs*NF-L, using anti-*hs*NF-L antibody, in wild-type HEK293T cells, 2-KO cell line #1, and 2-KO cell line #2. The apparent M_r, upon SDS/PAGE, of the 543-residue *hs*NF-L is ∼70 kDa. Lanes 4 through 6, same as in lanes 1 through 3, but using extracts from cells preincubated in the absence of FBS. (*D*) Same as in *C* but IB with anti-*hs*GAPDH antibody (loading control). (*E*) Same as in *C* but detection of *hs*NF-L using anti-*hs*NF-L antibody and chemiluminescence.

difference between the levels of *hs*NF-L in wild-type vs. 2-KO cells (Fig. 3 *C* and *D*; see also Fig. 3*E*). Thus, IB assays indicated an even stronger down-regulation of *hs*NF-L than the one suggested by MS data (*SI Appendix*, Fig. S13*A*).

In sum, the expression of *hs*NF-L and *hs*NF-M proteins was nearly completely abolished in 2-KO human cells, in contrast to robust expression of these proteins in wild-type cells (Fig. 3 *B–E* and *SI Appendix*, Fig. S13*A*). α-Internexin (encoded by *hsINA*) is present in some but not all neurofilaments. In contrast to *hs*NF-L and *hs*NF-M, α-internexin was increased by approximately twofold in 2-KO cells (*SI Appendix*, Fig. S12*A*). Thus, the nearly complete dependence of expression of *hs*NF-L and *hs*NF-M on the presence of *hs*UBR1/*hs*UBR2 (Fig. 3 *B–E* and *SI Appendix*, Fig. S13*A*) does not encompass all subunits of neurofilaments.

Repression in 2-KO Cells of NF-L and NF-M Takes Place Despite Up-Regulation of Their mRNAs. Remarkably, the disappearance or near disappearance of *hs*NF-L and *hs*NF-M in 2-KO cells (in contrast to their robust expression in wild-type cells) took place despite up-regulation by ∼1.7-fold and ∼1.2-fold, respectively, of *hsNF-L* (*hsNFEL*) and *hsNF-M* (*hsNFEM*) mRNAs in 2-KO cells (Fig. 3 *B–E* and *SI Appendix*, Fig. S13*A*). Thus, the near absence of *hs*NF-L and *hs*NF-M proteins in 2-KO cells could not have been caused by transcriptional repression of the corresponding genes or by destabilization of *hsNF-L* and *hsNF-M* mRNAs.

A parsimonious interpretation of these results is that the absence of the *hs*UBR1/*hs*UBR2 Ub ligases causes repression of translation of *hsNF-L* and *hsNF-M* mRNAs in 2-KO cells. In one verifiable model, a selective translational repression would be caused by metabolic stabilization (and therefore up-regulation) of a normally short-lived (and remaining to be identified) translational repressor(s) of *hsNF-L* and *hsNF-M* mRNAs in 2-KO cells. The postulated repressor(s), presumably an RNA-binding protein(s) that recognizes *hsNF-L* and *hsNF-M* mRNAs, is normally down-regulated through degradation by the *hs*UBR1/*hs*UBR2-mediated Arg/N-degron pathway. Consequently, this repressor(s) becomes long-lived in 2-KO cells, and its level increases strongly enough to shut off translation of (at least) *hsNF-L* and *hsNF-M* mRNAs. Work to verify this model is under way.

In contrast to *hs*NF-L and *hs*NF-M proteins, whose near disappearance in 2-KO cells takes place despite up-regulation of

their respective mRNAs in these cells (Fig. 3 *B–E* and *SI Appendix*, Fig. S13*A*), the near absence of *hs*DACH1 TF in 2-KO cells is accompanied by a 3.8-fold decrease of its mRNA (Fig. 3*A* and *SI Appendix*, Fig. S13*A*). Nevertheless, the observed down-regulation of *hs*DACH1 protein in 2-KO cells is much stronger than the down-regulation of *hsDACH1* mRNA, suggesting that an *hs*UBR1/*hs*UBR2-dependent translational repression, described in the context of *hs*NF-L and *hs*NF-M proteins, may also apply, at least in part, to regulation of *hs*DACH1.

Split-Ubiquitin Binding Assays. In this technique, two proteins are expressed in yeast as fusions to a Ct-half of Ub (C_{Ub}) and to its mutant Nt-half (N_{Ub}), respectively (Fig. 4*A*) (43, 60). An interaction between two examined proteins (which contain linked Ub halves) would reconstitute a Ub moiety from C_{Ub} and mutant N_{Ub}. Consequently, a C_{Ub}-containing test fusion would be cleaved by deubiquitylases at the last (Gly) residue of the reconstituted Ub moiety. This cleavage acts, through additional steps, as a set of assay's readouts (Fig. 4*A*) (43). They comprise, in particular, an induction of *scHIS3* and *scADE2* genes (Fig. 4*A*), thereby making possible growth assays on media that lack either histidine (His) or both His and adenine (Ade) (Fig. 4). Control experiments included IBs to examine expression of split-Ub fusions and also verification of the absence of autoactivation, i.e., that binding-positive fusions did not remain positive in split-Ub assays with just one of two fusions. The results described below passed all of these controls.

Having previously detected, in part through split-Ub assays, the binding of the stress-inducible bZIP-class *hs*ATF3 TF to an Nt-fragment of *hs*UBR1 (42), we examined here *hs*UBR1 interactions with two other TFs, the *hs*PREP1 TF and the glucocorticoid receptor (*hs*GR) TF, encoded by the *hsNR3C1* gene (Fig. 4). We tested *hs*PREP1 (*hs*PKNOX1), a homeodomain TF (61) (Fig. 4*B*), owing to a significant sequelogy between *hs*PREP1 and *S. cerevisiae sc*CUP9, a yeast transcriptional repressor. *sc*CUP9 is a key part of a circuit in which the conditional (regulated by short peptides) degradation of *sc*CUP9 by the Arg/N-degron pathway controls the rate of peptide import in yeast (see below) (2, 35, 36).

*hs*GR, a zinc-finger TF, is modulated by glucocorticoids and regulates processes that include immune responses as well as cell growth and differentiation (62). We tested *hs*GR for its binding to *hs*UBR1 (Fig. 4*C*) owing, in part, to MS-based data that the *hs*GR protein was up-regulated by 1.5-fold and 2.0-fold, respectively, in 2-KO cell lines #1 and #2, relative to wild-type cells. In addition, *hsGR* mRNA was up-regulated by 1.4-fold in 2-KO cell line #1, according to RNA-seq. These results are not mentioned in the corresponding protein and mRNA lists (*SI Appendix*, Figs. S4 and S12), inasmuch as the cited protein increases had been "ordered" according to data with 2-KO cell line #1 and had to be 2-fold or higher to make it into the list. We found later that *hs*GR protein is up-regulated by significantly more than 2-fold in 2-KO cells, in agreement with physical binding of an isoform of *hs*GR to an Nt-half of *hs*UBR1, as described below (Figs. 4*C* and 5).

***hs*PREP1 Transcription Factor Binds to the N-Terminal Fragment of *hs*UBR1 but Not to Full-Length *hs*UBR1.** Split-Ub assays revealed the binding of *hs*UBR1$^{1-1059}$, the 123-kDa Nt-fragment of the 200 kDa *hs*UBR1 E3, to the full-length 48-kDa *hs*PREP1 (Fig. 4*B*, row 2). In contrast, *hs*PREP1 did not bind to either full-length *hs*UBR1 or its 77-kDa Ct fragment (*hs*UBR1$^{1060-1749}$) (Fig. 4*B*, rows 1 through 4). The binding of a physiological substrate of UBR1 to its Nt-fragment but not to full-length UBR1 has been encountered earlier in two different settings.

First, *hs*ATF3, a bZIP TF, was found to interact, both in split-Ub assay and in another (conceptually different) binding assay, with the Nt-fragment of *hs*UBR1 but not with its full-length

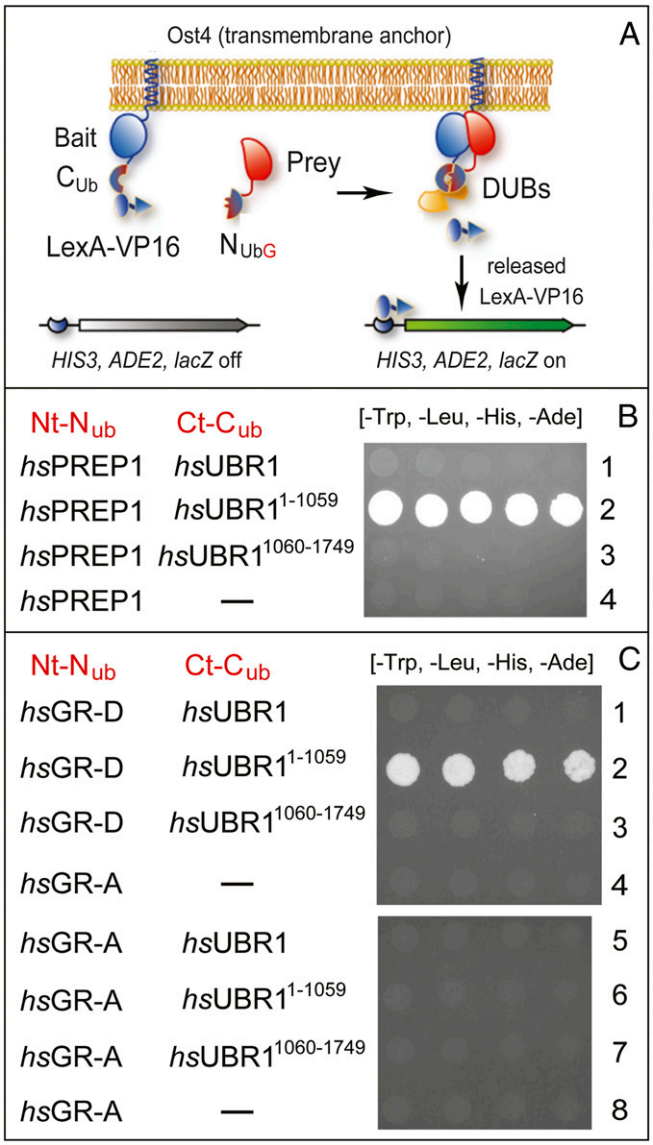

Fig. 4. Split-ubiquitin binding assays with transcription factors *hs*PREP1 and glucocorticoid receptor (*hs*GR) vs. *hs*UBR1 E3 ubiquitin ligase. (*A*) Design of split-Ub assays (also see the main text). (*B*) Row 1, *hs*PREP1 vs. full-length *hs*UBR1. Row 2, *hs*PREP1 vs. Nt-fragment of *hs*UBR1 (*hs*UBR1$^{1-1059}$). Row 3, *hs*PREP1 vs. Ct-fragment of *hs*UBR1 (*hs*UBR1$^{1060-1749}$). Row 4, *hs*PREP1 vs. vector alone. Note the binding of *hs*PREP1 solely to the Nt-fragment of *hs*UBR1. (*C*) See the main text and Fig. 5 for definitions and descriptions of the *hs*GR-D isoform. Row 1, *hs*GR-D vs. full-length *hs*UBR1. Row 2, *hs*GR-D vs. Nt-fragment of *hs*UBR1 (*hs*UBR1$^{1-1059}$). Row 3, *hs*GR-D vs. Ct-fragment of *hs*UBR1 (*hs*UBR1$^{1060-1749}$). Row 4, *hs*GR-D vs. vector alone. Row 5, *hs*GR-A vs. full-length *hs*UBR1. Row 6, *hs*GR-A vs. Nt-fragment of *hs*UBR1 (*hs*UBR1$^{1-1059}$). Row 7, *hs*GR-A vs. Ct-fragment of *hs*UBR1 (*hs*UBR1$^{1060-1749}$). Row 8, *hs*GR-A vs. vector alone.

counterpart (42). Second, *S. cerevisiae sc*CUP9 TF, a transcriptional repressor of a regulon that includes the *sc*PTR2 peptide importer, was found to bind, unconditionally, to the analogous Nt-fragment of *sc*UBR1, but would bind to full-length *sc*UBR1 only in the presence of dipeptides bearing destabilizing (type-1/2) Nt-residues (2, 35, 36). As shown previously, Nt-residues of such dipeptides can interact with two cognate-binding sites of full-length *sc*UBR1 (they are present in *hs*UBR1 as well; Fig. 1), thereby altering conformation of *sc*UBR1 and enabling its binding to the *sc*CUP9 repressor, followed by polyubiquitylation

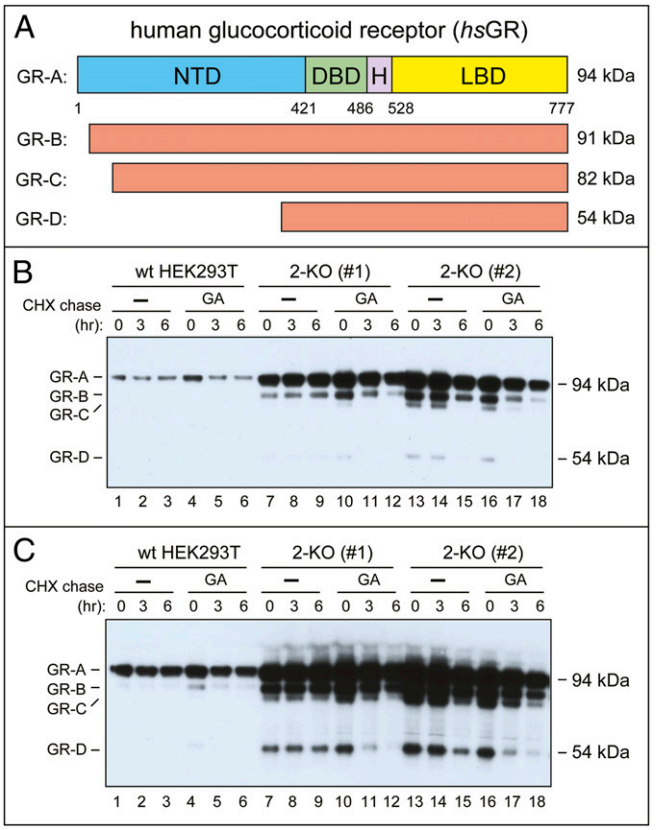

Fig. 5. Up-regulation of the *hs*GR transcription factor in 2-KO HEK293T cells. (*A*) Main *hs*GR isoforms (detailed terminology of *hs*GR isoforms is more complex than the one shown here) (ref. 62 and refs. therein). (*B*) Lanes 1 through 3, IB-based CHX chase, for 0, 3, and 6 h, with wild-type HEK293T cells, using anti-*hs*GR antibody that recognizes *hs*GR isoforms shown in *A*. Lanes 4 through 6, same as lanes 1 through 3, but wild-type cells were incubated with GA at the beginning and during chase (*SI Appendix, Materials and Methods*). Lanes 7 through 9, same as lanes 1 through 3, but with 2-KO cell line #1. Lanes 10 through 12, same as lanes 4 through 6, but with 2-KO cell line #1. Lanes 13 through 18, same as lanes 7 through 12, but with 2-KO cell line #2. (*C*) Same as in *B* but a longer chemiluminescence exposure.

and degradation of *sc*CUP9 (36). The resulting proteolysis-based *sc*UBR1-*sc*CUP9-*sc*PTR2 circuit, regulated by short peptides, enables yeast cells to "sense" extracellular peptides and to accelerate their uptake (2, 35, 36). Despite physiologically plausible analogies between the conditional binding of *sc*CUP9 to full-length *sc*UBR1 and the current disposition with human *hs*ATF3 and *hs*PREP1 (and with *hs*GR as well; see below), our binding assays did not suggest, so far, any "induction," by short peptides, of interactions between full-length *hs*UBR1 and either *hs*ATF3 or *hs*PREP1, which bind to the Nt-fragment of *hs*UBR1 but not to its full-length counterpart (Fig. 4*B*).

Isoform D of Glucocorticoid Receptor TF Binds to the N-Terminal Fragment of *hs*UBR1 but Not to Full-Length *hs*UBR1. Human *hs*GR, encoded by *hsNR3C1* and described above, exists in cells as a set of protein isoforms that include the major and largest (94 kDa) isoform *hs*GR-A, as well as smaller isoforms, including the 54 kDa *hs*GR-D (Fig. 5*A*). *hs*GR-A comprises the Nt domain, DNA-binding domain, hinge region, and the ligand-binding (glucocorticoid binding) domain (LBD) (Fig. 5*A*) (62).

Split-Ub assays revealed the binding of the Nt-fragment of *hs*UBR1 (*hs*UBR1$^{1-1059}$) to the smallest, 54-kDa isoform *hs*GR-D (Fig. 4*C*, row 2, and Fig. 5*A*). However, similarly to *hs*ATF3 and *hs*PREP1 TFs, the *hs*GR-D did not bind to full-length *hs*UBR1 (Fig. 4*C*, rows 1 through 4). In addition and remarkably, the largest isoform, *hs*GR-A, despite encompassing the entire *hs*GR-D isoform (Fig. 5*A*), did not bind to either full-length *hs*UBR1 or its fragments (Fig. 4*C*, rows 5 through 8; compare with rows 1 through 4). Thus, the interaction, under the conditions of split-Ub assays, between *hs*GR and *hs*UBR1 was "restricted" for both ligands, in that the binding occurred solely between the Nt-fragment of *hs*UBR1 and the *hs*GR-D isoform, but was not observed (for any form of *hs*UBR1) with the largest isoform, hsGR-A (Figs. 4*C* and 5*A*).

Up-Regulation of Glucocorticoid Receptor in 2-KO Cells. Cycloheximide (CHX)-based chase-degradation assays with untagged, endogenous *hs*GR used IB assays, anti-*hs*GR antibody, and wild-type HEK293T cells vs. 2-KO cells (Fig. 5). *hs*GR-A, the largest *hs*GR isoform, was largely stable during 6-h CHX chase, but became unstable in the presence of geldanamycin (GA), an inhibitor of the HSP90 chaperone (Fig. 5*B*, lanes 1 through 6). The latter finding was in agreement with *hs*GR being a client of HSP90, which assists the folding of *hs*GR and partially protects it from degradation (62). Remarkably, the steady-state levels of endogenous *hs*GR-A were at least 5-fold higher in both 2-KO cell lines, #1 and #2, than in wild-type cells (Fig. 5*B*, lanes 7 through 18; compare with lanes 1 through 6).

In addition, a higher-sensitivity detection (a longer chemiluminescence exposure) revealed, in 2-KO cell lines, a greatly increased level of *hs*GR-D, the smallest *hs*GR isoform (Fig. 5*C*), the one that has been found, above, to interact with the Nt-half of *hs*UBR1 (Fig. 4*C*). While undetectable in wild-type HEK293T cells even at the highest sensitivity of IB assays (Fig. 5*C*, lanes 1 through 6), the *hs*GR-D isoform was readily detectable and stable during a 6-h chase in the 2-KO cell line #1 (Fig. 5*C*, lanes 7 through 9), while being also up-regulated but less stable in the 2-KO cell line #2 (Fig. 5*C*, lanes 13 through 15).

Interestingly, the *hs*GR-D isoform became short-lived, in both 2-KO cell lines, in the presence of GA, despite the absence in these cells of both the *hs*UBR1 and *hs*UBR2 Ub ligases (Fig. 5*C*, lanes 10 through 12 and 16 through 18). Thus, the bulk of the Arg/N-degron pathway (its *hs*UBR1/*hs*UBR2 part) is not required for the degradation of either *hs*GR-A or *hs*GR-D isoforms (the latter isoform binds to the Nt-fragment of *hs*UBR1) that lost their protection by the HSP90 chaperone, in agreement with the known targeting of many specific TFs by more than one proteolytic pathway (63).

A parsimonious but not the only possible interpretation of these results is that the strong increase of both *hs*GR-A and *hs*GR-D isoforms (and other, "intermediate" *hs*GR isoforms as well) in 2-KO HEK293T cells (Fig. 5*C*) stems, at least in part, from a metabolic stabilization of these isoforms in the absence of *hs*UBR1/*hs*UBR2. The apparent stabilization of the *hs*GR-D isoform in this genetic background (Fig. 5*C*, lanes 7 through 9) suggests that the relevant (*hs*UBR1/*hs*UBR2 targeted) degron of *hs*GR resides in its LBD, which occupies the bulk of *hs*GR-D isoform (Fig. 5*A*).

In this interpretation, the largest (*hs*GR-A) isoform, the one that did not bind to any form of *hs*UBR1, in contrast to the *hs*GR-D isoform (Fig. 4*C*), is nevertheless recognized and destroyed by the Arg/N-degron pathway in vivo, in wild-type cells, similarly to *hs*GR-D. If so, a specific reason for the reproducible absence of binding of *hs*GR-A to any form of *hs*UBR1 in split-Ub assays, in contrast to the binding of *hs*GR-D to the Nt-half of *hs*UBR1 (Fig. 4*C*), remains to be understood. One possibility, to be addressed in future studies of *hs*GR vs. the Arg/N-degron pathway, is that this pathway mediates an early degradation of newly formed *hs*GR molecules, before their

conformational maturation and/or interaction with other proteins, including *hs*GR itself. Yet another unknown in this setting, to be addressed by future experiments, is the possibility that a strong up-regulation of all isoforms of *hs*GR in 2-KO cells (Fig. 5*C*) may be caused, in part, by effects of the *hs*UBR1/*hs*UBR2 ablation on, for example, the efficacy of translation of *hsGR* mRNAs. In sum, while it is highly likely that at least *hs*GR-D (and possibly all isoforms of *hs*GR) are targeted by the Arg/N-degron pathway, the details of this circuit and whether the role of *hs*UBR1/*hs*UBR2 is solely degradative or has nonproteolytic aspects as well, remain to be understood.

Concluding Remarks. It is still an unproven assumption that all functions of the Arg/N-degron pathway (Fig. 1) involve, in the end, the destruction of a targeted protein substrate, as distinguished, for example, from a nondegradative modification of substrate through its ubiquitylation by this pathway (2). On that assumption, the remarkably large alterations in the levels of some mRNAs and proteins that result from genetic ablation of the *hs*UBR1/*hs*UBR2 E3 N-recognins in human HEK293T cells (Figs. 2 and 3 and *SI Appendix*, Figs. S2–S13) are likely to be caused, at least in part, by metabolic stabilization (and therefore up-regulation) of specific TFs (repressors and/or activators) in 2-KO mutant cells that lack *hs*UBR1/*hs*UBR2. One such "promoter-based" model, for the strongly up-regulated *hsADRB2* mRNA and its encoded protein, is described in this paper (Fig. 2 *B–D* and *SI Appendix*, Fig. S8). Analogous and verifiable models can also be developed, using the same logic, for other *hs*UBR1/*hs*UBR2-impacted genes described in the present study.

Our earlier work identified *hs*ATF3, a stress-inducible TF that regulates hundreds of genes, as a short-lived substrate of the Arg/N-degron pathway in ref. 42. In the present study, we identified another major TF, the glucocorticoid receptor (*hs*GR), as a second TF that interacts with *hs*UBR1 in split-Ub assays and is strongly influenced, in ways described above, by the ablation of *hs*UBR1/*hs*UBR2 (Figs. 4*C* and 5). A TF called *hs*PREP1was also found to bind to *hs*UBR1 of the Arg/N-degron pathway (Fig. 4*B*), suggesting that *hs*PREP1 is yet another human TF that is impacted, through degradation and/or otherwise, by this proteolytic system.

All three TFs, while binding to the Nt-half of the 200-kDa *hs*UBR1 E3, did not interact in split-Ub assays with full-length *hs*UBR1 (Fig. 4). This binding pattern was first encountered in studies of *S. cerevisiae sc*CUP9, a transcriptional repressor, which can bind unconditionally to the Nt-half of *sc*UBR1 but would bind to full-length *sc*UBR1 only in the presence of short peptides that bear destabilizing Nt residues and thereby can convert *sc*UBR1, upon its binding to these peptides, into a conformer that can interact with *sc*CUP9. As described in more detail above, these properties of *sc*CUP9-*sc*UBR1 interactions underlie the ability of the Arg/N-degron pathway to control peptide transport in yeast, through the regulated (by short peptides) degradation of the *sc*CUP9 repressor (2, 35, 36). It remains to be determined whether a human TF, such as, for example, *hs*PREP1 (it is sequelogous to *sc*CUP9) may regulate peptide transport in mammals by being a conditionally short-lived substrate of the Arg/N-degron pathway.

Given that three TFs of different structures were found to bind to the Nt-half of *hs*UBR1 in split-Ub assays (*hs*ATF3 is a bZIP TF, *hs*GR is a zinc-finger TF, and *hs*PREP1 is a homeodomain TF) (Fig. 4) (42), it would be illuminating to identify all or most human TFs (~1,600 distinct TFs total) (63) that are bona fide in vivo substrates of the Arg/N-degron pathway. Specific degrons (binding sites) that *hs*UBR1 recognizes in the three TFs remain to be determined as well. Yet another vista opened up by the present study (and discussed above) is the function of the Arg/N-degron pathway as a regulator of translation of specific mRNAs, such as those that encode the NF-L and NF-M subunits of neurofilaments (Fig. 3 and *SI Appendix*, Fig. S13*A*).

A large number of mRNAs and proteins that were found to be either significantly or very strongly up-regulated or down-regulated in 2-KO human cells that lacked *hs*UBR1/*hs*UBR2 has greatly exceeded our ability to follow up and explore these findings in the present study. Consequently, these detailed results (Figs. 2–5 and *SI Appendix*, Figs. S2–S13) are likely to serve for a long time as sources of mRNA and protein leads for analyzing circuits that involve the Arg/N-degron pathway. This multifunctional proteolytic system has emerged as a regulator of specific mammalian genes, in part through conditional targeting of TFs that include ATF3, GR, and PREP1.

Materials and Methods

For further information, see *SI Appendix, Materials and Methods*.

RNA-Seq Analyses. RNA-seq was carried out with RNA preparations from wild-type vs. 2-KO (*UBR1*$^{-/-}$ *UBR2*$^{-/-}$) HEK293T cell lines using methods described in *SI Appendix, Materials and Methods*.

Quantitative Mass Spectrometric (TMT-SPS-MS3) Protein Analyses. MS-based analyses of extracts from wild-type and 2-KO HEK293T cells employed the TMT-SPS-MS3 technique, described in *SI Appendix, Materials and Methods*.

Cell Viability and Proliferation Assay. Cell viability and proliferation were assayed using the Trypan Blue exclusion test, as described in *SI Appendix, Materials and Methods*.

Cell Toxicity Assay with Dimethyloxalylglycine. This assay, which uses DMOG to probe relative in vivo levels of the *hs*MCT2 transporter, is described in *SI Appendix, Materials and Methods*.

Immunoblotting and Chase-Degradation Assays. IB analyses and chase-degradation assays were carried out largely as described previously (23, 26) and in *SI Appendix, Materials and Methods*.

Split-Ubiquitin Assay. A version of split-Ub binding assay (Fig. 4*A*) (43) was carried out in *S. cerevisiae* as described previously (26, 42, 60) and in *SI Appendix, Materials and Methods*. Standard techniques were used for construction of *S. cerevisiae* strains and transformation by DNA.

Data Availability. All relevant data are included in the article and supporting information.

ACKNOWLEDGMENTS. We are grateful to I. Antoshechkin for RNA-seq analyses. T.T.M.V. and A.V. thank current and former members of the A.V. laboratory for their advice and assistance. D.C.M. and S.P.G. thank J. Paulo for assistance with mass spectrometry experiments. This work was supported by NIH grants 1R01DK039520 and 1R01GM031530 (A.V.) and R01GM067945 (S.P.G.).

1. A. Hershko, A. Ciechanover, A. Varshavsky, The ubiquitin system. *Nat. Med.* **6**, 1073–1081 (2000).
2. A. Varshavsky, N-degron and C-degron pathways of protein degradation. *Proc. Natl. Acad. Sci. U.S.A.* **116**, 358–366 (2019).
3. D. Finley, H. D. Ulrich, T. Sommer, P. Kaiser, The ubiquitin-proteasome system of Saccharomyces cerevisiae. *Genetics* **192**, 319–360 (2012).
4. V. Vittal, M. D. Stewart, P. S. Brzovic, R. E. Klevit, Regulating the regulators: Recent revelations in the control of E3 ubiquitin ligases. *J. Biol. Chem.* **290**, 21244–21251 (2015).
5. C. Pohl, I. Dikic, Cellular quality control by the ubiquitin-proteasome system and autophagy. *Science* **366**, 818–822 (2019).
6. D. Balchin, M. Hayer-Hartl, F. U. Hartl, In vivo aspects of protein folding and quality control. *Science* **353**, aac4354 (2016).
7. N. Zheng, N. Shabek, Ubiquitin ligases: Structure, function, and regulation. *Annu. Rev. Biochem.* **86**, 129–157 (2017).
8. A. Schweitzer *et al.*, Structure of the human 26S proteasome at a resolution of 3.9 Å. *Proc. Natl. Acad. Sci. U.S.A.* **113**, 7816–7821 (2016).
9. J. A. M. Bard *et al.*, Structure and function of the 26S proteasome. *Annu. Rev. Biochem.* **87**, 697–724 (2018).
10. D. Finley, M. A. Prado, The proteasome and its network: Engineering for adaptability. *Cold Spring Harb. Perspect. Biol.* **12**, a033985 (2020).

11. A. Bachmair, D. Finley, A. Varshavsky, In vivo *h*alf-life of a protein is a function of its amino-terminal residue. *Science* **234**, 179–186 (1986).
12. R. T. Timms, I. Koren, Tying up loose ends: The N-degron and C-degron pathways of protein degradation. *Biochem. Soc. Trans.* **48**, 1557–1567 (2020).
13. R.-G. Hu *et al*., The N-end rule pathway as a nitric oxide sensor controlling the levels of multiple regulators. *Nature* **437**, 981–986 (2005).
14. M. J. Lee *et al*., RGS4 and RGS5 are in vivo substrates of the N-end rule pathway. *Proc. Natl. Acad. Sci. U.S.A.* **102**, 15030–15035 (2005).
15. A. Varshavsky, The N-end rule pathway and regulation by proteolysis. *Protein Sci.* **20**, 1298–1345 (2011).
16. T. Tasaki, S. M. Sriram, K. S. Park, Y. T. Kwon, The N-end rule pathway. *Annu. Rev. Biochem.* **81**, 261–289 (2012).
17. R. Ree, S. Varland, T. Arnesen, Spotlight on protein N-terminal acetylation. *Exp. Mol. Med.* **50**, 1–13 (2018).
18. M. J. Holdsworth, J. Vicente, G. Sharma, M. Abbas, A. Zubrycka, The plant N-degron pathways of ubiquitin-mediated proteolysis. *J. Integr. Plant Biol.* **62**, 70–89 (2020).
19. C. S. Hwang, A. Shemorry, A. Varshavsky, N-terminal acetylation of cellular proteins creates specific degradation signals. *Science* **327**, 973–977 (2010).
20. A. Shemorry, C. S. Hwang, A. Varshavsky, Control of protein quality and stoichiometries by N-terminal acetylation and the N-end rule pathway. *Mol. Cell* **50**, 540–551 (2013).
21. S. J. Chen, X. Wu, B. Wadas, J.-H. Oh, A. Varshavsky, An N-end rule pathway that recognizes proline and destroys gluconeogenic enzymes. *Science* **355**, 366 (2017).
22. S. Qiao *et al*., Interconversion between anticipatory and active GID E3 ubiquitin ligase conformations via metabolically driven substrate receptor assembly. *Mol. Cell* **77**, 150–163.e9 (2020).
23. K. I. Piatkov, C. S. Brower, A. Varshavsky, The N-end rule pathway counteracts cell death by destroying proapoptotic protein fragments. *Proc. Natl. Acad. Sci. U.S.A.* **109**, E1839–E1847 (2012).
24. C. S. Brower, K. I. Piatkov, A. Varshavsky, Neurodegeneration-associated protein fragments as short-lived substrates of the N-end rule pathway. *Mol. Cell* **50**, 161–171 (2013).
25. R. F. Shearer, M. Iconomou, C. K. Watts, D. N. Saunders, Functional roles of the E3 ubiquitin ligase UBR5 in cancer. *Mol. Cancer Res.* **13**, 1523–1532 (2015).
26. J. H. Oh, J. Y. Hyun, A. Varshavsky, Control of Hsp90 chaperone and its clients by N-terminal acetylation and the N-end rule pathway. *Proc. Natl. Acad. Sci. U.S.A.* **114**, E4370–E4379 (2017).
27. Y. D. Yoo *et al*., N-terminal arginylation generates a bimodal degron that modulates autophagic proteolysis. *Proc. Natl. Acad. Sci. U.S.A.* **115**, E2716–E2724 (2018).
28. N. Masson *et al*., Conserved N-terminal cysteine dioxygenases transduce responses to hypoxia in animals and plants. *Science* **365**, 65–69 (2019).
29. X. Gao, J. Yeom, E. A. Groisman, The expanded specificity and physiological role of a widespread N-degron recognin. *Proc. Natl. Acad. Sci. U.S.A.* **116**, 18629–18637 (2019).
30. R. T. Timms *et al*., A glycine-specific N-degron pathway mediates the quality control of protein N-myristoylation. *Science* **365**, eaaw4912 (2019).
31. J. S. Park *et al*., Structural analyses on the deamidation of N-terminal Asn in the human N-degron pathway. *Biomolecules* **10**, 163 (2020).
32. M. K. Kim, S. J. Oh, B. G. Lee, H. K. Song, Structural basis for dual specificity of yeast N-terminal amidase in the N-end rule pathway. *Proc. Natl. Acad. Sci. U.S.A.* **113**, 12438–12443 (2016).
33. D. A. Dougan, A. Varshavsky, Understanding the Pro/N-end rule pathway. *Nat. Chem. Biol.* **14**, 415–416 (2018).
34. J. H. Oh, J. Y. Hyun, S. J. Chen, A. Varshavsky, Five enzymes of the Arg/N-degron pathway form a targeting complex: The concept of superchanneling. *Proc. Natl. Acad. Sci. U.S.A.* **117**, 10778–10788 (2020).
35. G. C. Turner, F. Du, A. Varshavsky, Peptides accelerate their uptake by activating a ubiquitin-dependent proteolytic pathway. *Nature* **405**, 579–583 (2000).
36. F. Du, F. Navarro-Garcia, Z. Xia, T. Tasaki, A. Varshavsky, Pairs of dipeptides synergistically activate the binding of substrate by ubiquitin ligase through dissociation of its autoinhibitory domain. *Proc. Natl. Acad. Sci. U.S.A.* **99**, 14110–14115 (2002).
37. D. J. Gibbs, M. J. Holdsworth, Every breath you take: New insights into plant and animal oxygen sensing. *Cell* **180**, 22–24 (2020).
38. A. J. Chui *et al*., N-terminal degradation activates the NLRP1B inflammasome. *Science* **364**, 82–85 (2019).
39. A. Varshavsky, 'Spalog' and 'sequelog': Neutral terms for spatial and sequence similarity. *Curr. Biol.* **14**, R181–R183 (2004).
40. M. Zenker *et al*., Deficiency of UBR1, a ubiquitin ligase of the N-end rule pathway, causes pancreatic dysfunction, malformations and mental retardation (Johanson-Blizzard syndrome). *Nat. Genet.* **37**, 1345–1350 (2005).
41. J. Y. An *et al*., Impaired neurogenesis and cardiovascular development in mice lacking the E3 ubiquitin ligases UBR1 and UBR2 of the N-end rule pathway. *Proc. Natl. Acad. Sci. U.S.A.* **103**, 6212–6217 (2006).
42. T. T. M. Vu, A. Varshavsky, The ATF3 transcription factor is a short-lived substrate of the Arg/N-degron pathway. *Biochemistry* **59**, 2796–2812 (2020).
43. N. Johnsson, A. Varshavsky, Split ubiquitin as a sensor of protein interactions in vivo. *Proc. Natl. Acad. Sci. U.S.A.* **91**, 10340–10344 (1994).
44. K. Van der Berge *et al*., RNA sequencing data: Hitchhiker's guide to expression analysis. *Annu. Rev. Biomed. Data Sci.* **2**, 139–173 (2019).
45. J. Navarrete-Perea, Q. Yu, S. P. Gygi, J. A. Paulo, Streamlined tandem mass tag (SL-TMT) protocol: An efficient strategy for quantitative (phospho)proteome profiling using tandem mass tag-synchronous precursor selection-MS3. *J. Proteome Res.* **17**, 2226–2236 (2018).
46. Y. Daaka, L. M. Luttrell, R. J. Lefkowitz, Switching of the coupling of the beta2-adrenergic receptor to different G proteins by protein kinase A. *Nature* **390**, 88–91 (1997).
47. A. Jaeger, S. Fritschka, S. Ponsuksili, K. Wimmers, E. Muráni, Identification and functional characterization of cis-regulatory elements controlling expression of the porcine ADRB2 gene. *Int. J. Biol. Sci.* **11**, 1006–1015 (2015).
48. S. W. Bahouth, M. J. Beauchamp, K. N. Vu, Reciprocal regulation of beta(1)-adrenergic receptor gene transcription by Sp1 and early growth response gene 1: Induction of EGR-1 inhibits the expression of the beta(1)-adrenergic receptor gene. *Mol. Pharmacol.* **61**, 379–390 (2002).
49. L. O'Connor, J. Gilmour, C. Bonifer, The Role of the ubiquitously expressed transcription factor Sp1 in tissue-specific transcriptional regulation and in disease. *Yale J. Biol. Med.* **89**, 513–525 (2016).
50. A. P. Halestrap, The SLC16 gene family–Structure, role and regulation in health and disease. *Mol. Aspects Med.* **34**, 337–349 (2013).
51. L. Fets *et al*., MCT2 mediates concentration-dependent inhibition of glutamine metabolism by MOG. *Nat. Chem. Biol.* **14**, 1032–1042 (2018).
52. J. Schödel, P. J. Ratcliffe, Mechanisms of hypoxia signalling: New implications for nephrology. *Nat. Rev. Nephrol.* **15**, 641–659 (2019).
53. W. G. Kaelin Jr, The VHL tumor suppressor gene: Insights into oxygen sensing and cancer. *Trans. Am. Clin. Climatol. Assoc.* **128**, 298–307 (2017).
54. C. D. Jayewickreme, R. A. Shivdasani, Control of stomach smooth muscle development and intestinal rotation by transcription factor BARX1. *Dev. Biol.* **405**, 21–32 (2015).
55. A. K. Lee, P. R. Potts, A comprehensive guide to the MAGE family of ubiquitin ligases. *J. Mol. Biol.* **429**, 1114–1142 (2017).
56. V. M. Popov *et al*., The Dachshund gene in development and hormone-responsive tumorigenesis. *Trends Endocrinol. Metab.* **21**, 41–49 (2010).
57. B. G. Szaro, M. J. Strong, Post-transcriptional control of neurofilaments: New roles in development, regeneration and neurodegenerative disease. *Trends Neurosci.* **33**, 27–37 (2010).
58. A. Yuan, M. V. Rao, Veeranna, R. A. Nixon, Neurofilaments and neurofilament proteins in health and disease. *Cold Spring Harb. Perspect. Biol.* **9**, a018309 (2017).
59. G. Shaw, S. Morse, M. Ararat, F. L. Graham, Preferential transformation of human neuronal cells by human adenoviruses and the origin of HEK 293 cells. *FASEB J.* **16**, 869–871 (2002).
60. S. M. Gisler *et al*., Monitoring protein-protein interactions between the mammalian integral membrane transporters and PDZ-interacting partners using a modified split-ubiquitin membrane yeast two-hybrid system. *Mol. Cell. Proteomics* **7**, 1362–1377 (2008).
61. F. Blasi, C. Bruckmann, D. Penkov, L. Dardaei, A tale of TALE, PREP1, PBX1, and MEIS1: Interconnections and competition in cancer. *BioEssays* **39**, 1600245 (2017).
62. E. R. Weikum, M. T. Knuesel, E. A. Ortlund, K. R. Yamamoto, Glucocorticoid receptor control of transcription: Precision and plasticity via allostery. *Nat. Rev. Mol. Cell Biol.* **18**, 159–174 (2017).
63. S. A. Lambert *et al*., The human transcription factors. *Cell* **172**, 650–665 (2018).